QJEGH

Technical note

Quarterly Journal of Engineering Geology and Hydrogeology

Published Online First

https://doi.org/10.1144/qjegh2020-050

In situ seepage testing method for fractured zones of rock mass

Sihong Liu[1], Siyuan Xu[1]* and Bin Zhou[2]

[1] College of Water Conservancy and Hydropower Engineering, Hohai University, Nanjing 210098, People's Republic of China
[2] Greenland Holdings Corporation Limited, Shanghai 200023, People's Republic of China
SX, 0000-0003-2462-0418
* Correspondence: i@siyuanxu.com

Abstract: The permeability characteristics of rock mass discontinuities are important in the stability of hydropower station projects. We propose a large-scale *in situ* seepage testing method and use this method to test gently dipping bedding faults (C3 zone) and steep faults (F14) in a hydropower station construction field in China. The *in situ* test results are compared with those of both undisturbed and reconstituted specimens. The comparison indicates that the largest critical hydraulic gradient and the smallest seepage permeability coefficient are obtained via *in situ* tests because they are performed under stress states that simulate the natural stress of the surrounding rock mass. The natural stress of the surrounding rock mass cannot be reflected in tests of undisturbed and reconstituted specimens.

Received 29 February 2020; **revised** 25 July 2020; **accepted** 27 July 2020

The Baihetan hydropower project is located on the Jinsha River and has a total installed capacity of 1600 MW. It is the second largest hydropower station currently under construction in China. A concrete double-curvature arch dam with a height of 289 m will ultimately be built. Emeishan basalt rocks, which contain various rock mass discontinuities (including bedding fault zones, small faults and fractures) underlie the dam site (Fig. 1). The rock mass discontinuities can be roughly classified based on their inclination into gently dipping bedding fault zones and steep faults (Afrouz 1992). Before the construction of the dam began, most of the rock mass discontinuities were well above the groundwater or river level. The water pressure within the rock mass discontinuities will increase significantly after the completion of the project and impounding of the reservoir. This will lead to two adverse effects on the project: the leakage of reservoir water through the rock mass discontinuities (Gutiérrez *et al.* 2015) and rock mass discontinuity seepage deformation failures. The latter problem could cause the subsequent failure of the dam foundations and abutments (Sivakumar *et al.* 2018). The hydraulic properties of the rock mass discontinuities are therefore crucial to the safety of the Baihetan project.

The hydraulic properties of rock mass discontinuities are currently determined primarily via laboratory or borehole water pressure tests and field seepage tests. For example, Sato and Kuwano (2015) conducted one-dimensional laboratory seepage tests and found that the potential for hydraulic failure was governed by the properties of the material (e.g. the gradation curve and pore size). Laboratory seepage tests have the advantage of being easy to perform, but the reliability of the test results depends on the size of the specimen and the sampling location. Small specimens are not representative as a result of the lack of realistic rock discontinuity network modelling (Huang *et al.* 2019, 2020*a*, *b*), whereas large specimens are difficult to handle (Cosenza *et al.* 1999; Rochim *et al.* 2017). Small-scale measurements usually yield lower hydraulic conductivities than large-scale hydraulic tests (Nastev *et al.* 2004).

Sampling in the field will inevitably disturb the rock mass discontinuities (Min *et al.* 2004). Borehole water pressure tests mainly include the single-hole packer test, the three-section water pressure test and the cross-hole test. The single-hole packer test proposed by Louis and Maini (1970) is commonly used for relatively isotropic rock masses. However, its application is sometimes limited because it cannot provide sufficient pressure to simulate deep fracture stress states. To overcome this shortcoming, Louis (1972) proposed a three-section water pressure testing method, which can provide the permeability tensor when three sets of orthogonal fractures exist in a rock mass. However, this testing method is invalid if there are more than three sets of fractures in a rock mass or if the three fractures are not orthorhombic. In this case, Hsieh *et al.* (1985) proposed a cross-hole testing method that can determine the local permeability tensor of a rock mass even without a knowledge of the main direction of fracture development. Several extra monitoring wells must be drilled for the cross-hole testing method of Hsieh *et al.* (1985) and the theoretical interpretation of the test is complex (Yamaguchi *et al.* 1997). Borehole water pressure tests are usually conducted in boreholes deeper than 5 m and the test results reflect the average permeability of the fractured rock mass over a relatively wide range (Misstear *et al.* 2006; Mehr and Raeisi 2018).

Field seepage tests, which are usually conducted in adits, are probably the best approach to investigating the hydraulic properties of rock mass discontinuities (Cook 2000). Zhou *et al.* (1999) conducted adit sonic wave hole infiltration tests on the fractured rock mass at the Xiluodu hydropower station to obtain the permeability coefficient of the fractured rock mass. Jiang *et al.* (2007) introduced a high-pressure *in situ* seepage test method and discussed the seepage failure characteristics of hydraulic fracturing zones in rock mass discontinuities. Feng *et al.* (2012) performed field seepage tests on a broken rock mass on the left bank of the Xiangjiaba hydropower project to determine the permeability coefficients and seepage gradients.

We introduce here an *in situ* rock mass discontinuity seepage testing method in which the stress environment of the test block approaches natural conditions and the large test block is more representative of rock mass discontinuities. We present examples of the application of this test to the Baihetan dam site.

In situ seepage testing method

Figure 2 shows the principle of the *in situ* rock mass discontinuity seepage test. The system consists of a water supply, a compression

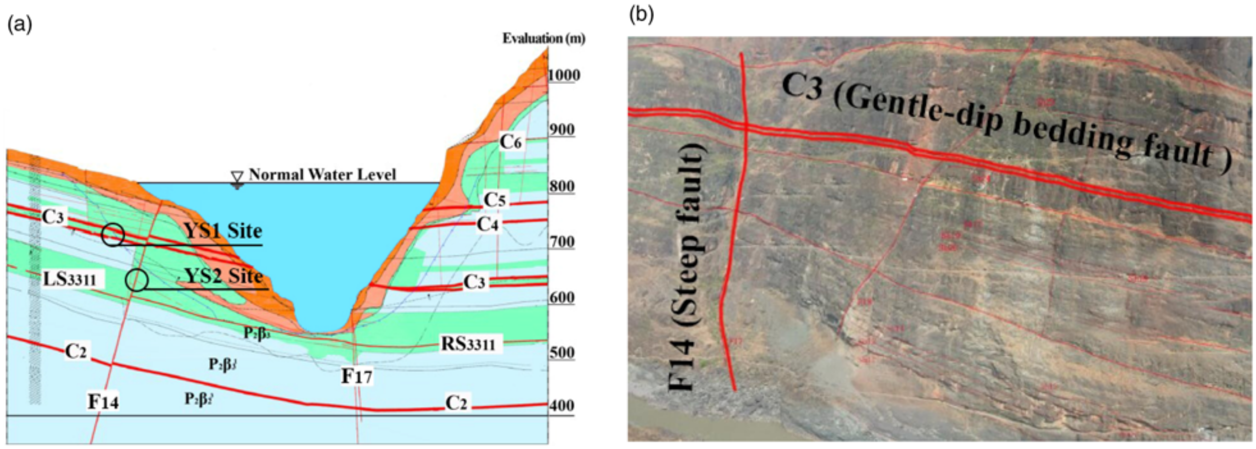

Fig. 1. Rock mass discontinuities at the Baihetan project dam site. (**a**) Geological profile along the axis of the dam. (**b**) Photograph of a rock mass discontinuity.

system, a pressure regulator, a pressure stabilization system and a measuring instrument. Using the compression system, the head of water from a tank is increased to the rated maximum of the centrifugal pump. Then, using a pressure regulator and pressure stabilization system, the water head is regulated to a pre-set value h_0 at the inlet of the test block. When the pressurized water flows through the test block, the water temperature is recorded and the changes in water pressure within the test block are measured using five piezometric tubes. The water flowing out of the test block is returned to the tank via a pipe so that it can be re-used. The inlet water pressure is gradually increased and applied to the test block through the pressure regulator and pressure stabilization system. At each inlet water pressure, the measurement continues until the outlet flow per unit of time is stabilized.

We used a single-suction, multi-stage centrifugal pump as the compression system. This provided a maximum water head of 350 m and a water flow-rate of 2.08 L s^{-1}. The pressure regulator and pressure stabilization systems were assembled in the field (Fig. 3). The pressure regulator system had three water flow paths for regulating three different ranges of water pressure (Fig. 4). Path A controlled the water pressure between 0.0 and 0.3 MPa via three pressure-reducing valves (RV1–RV3) and four stop valves (SV1–SV4). Path B controlled the water pressure between 0.3 and 1.0 MPa via two reducing valves (RV1 and RV2) and three stop valves (SV1, SV2 and SV5). Path C controlled the water pressure between 1.0 and 3.5 MPa via reducing valve RV1 and stop valves SV1 and SV6. The pressure stabilization system, which consists of two pressure vessels reinforced with three 8 mm diameter stirrups, was designed to eliminate the pulsing of high-pressure water from the centrifugal pump. Five piezometric tubes were installed in the test block to measure the water pressure along the seepage path.

Figures 5 and 6 show schematic views of the gently dipping bedding fault zones and steep faults, respectively. The tests were performed in adits. Because the rock mass surrounding the fault was compact, slightly weathered or fresh tuff, it was considered to be nearly impermeable. For the gently dipping bedding fault zones, the intact rock mass formed the upper and lower parts of the test block and the two lateral sides (the inlet and outlet) of the test block were surrounded by *c.* 50 cm of thick reinforced concrete. To prevent contact leakage between the reinforced concrete and the test block, a layer of plastic clay (*c.* 5 cm thick) was placed on the two side surfaces of the block before casting the reinforced concrete. For the steep faults, the two lateral sides of the test block were intact rock mass and the upper and lower parts of the block were isolated with reinforced concrete. The inlet and outlet of the test block were sealed with reinforced concrete. A 30 cm thick filter consisting of sandy pebbles (maximum grain size $d_{max} = 2$ cm) was placed between the reinforced concrete and the test block to prevent damage to the test block by pressurized water.

In situ seepage tests

We present two examples of the application of the *in situ* seepage test to a gently dipping bedding fault zone (C_3) and a steep fault (F_{14}) at the Baihetan dam site. The bedding fault zone (C_3) is located at an elevation of 725–735 m and has a thickness of 10–30 cm. This zone consists of fractured tuff and is filled with gravel, debris and some mud. It has a natural void ratio ranging from 0.25 to 0.39. Figure 7 shows the gradation of the filling materials within this zone, which has the characteristics $d_{max} = 60$ mm, $d_{50} = 0.1$ mm and $C_u = 60$. As shown in Figure 1, zone $C_3$is below the level of water in the reservoir and therefore may be one of the main leakage passages. The steep fault (F_{14}) is a fractured rock with breccia and gravel in its voids and has an average width of 43 cm. It is relatively dense with a natural void ratio of *c.* 0.15. The grains in F_{14} are relatively uniform with a coefficient of uniformity $C_u = 4$. The grain sizes range from 4

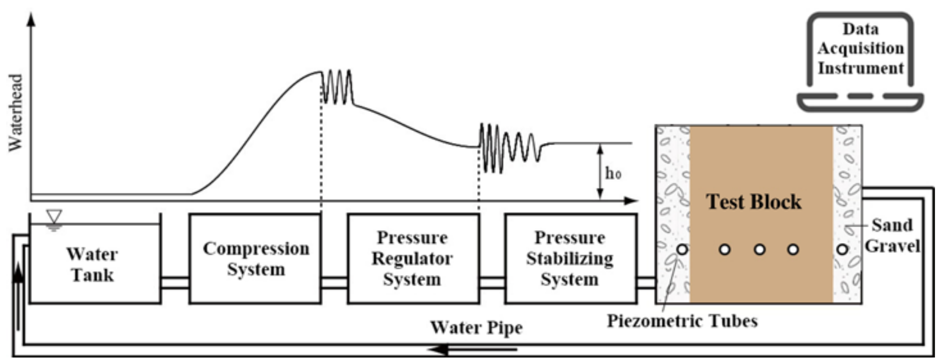

Fig. 2. Principle of the *in situ* seepage test.

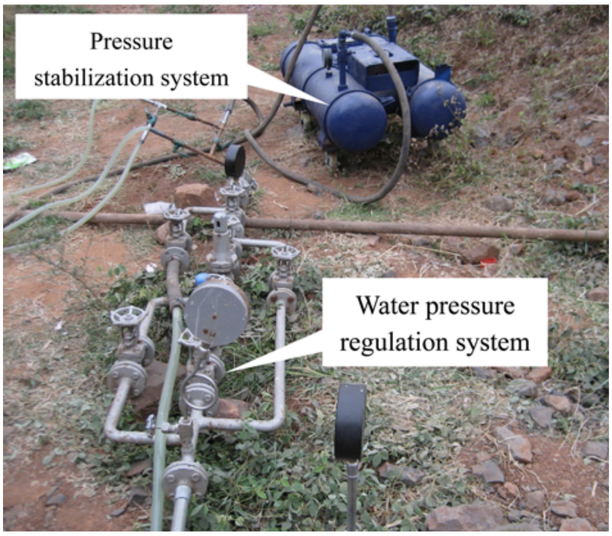

Fig. 3. Photograph of the regulation and pressure stabilization systems.

to 30 mm and fine grains (d<0.1 mm) make up <5% of the material (Fig. 7).

Test procedures

The test procedures included the preparation and saturation of a test block, the application of seepage pressure to the test block and the acquisition of seepage pressure and flow-rate information. The two application examples were almost the same, except for the preparation of the test block (Figs 5 and 6).

The *in situ* tests of the gently dipping bedding fault zone (C_3) and the steep fault (F_{14}) are denoted YS1 and YS2, respectively. Figure 5 shows that three branch adits were excavated to prepare the YS1 test block. Adits A and B were perpendicular to the main adit and the connection adit was parallel to the main adit. Two branch adits, one perpendicular to the main adit and the other parallel, were excavated to prepare the YS2 test block (Fig. 6). All the branch adits were 2 m wide, 2.5 m high and 4.5 m deep. The YS1 and YS2 test blocks had the same seepage length of 200 cm, whereas the seepage cross-sections were 200 cm × 26 cm and 200 cm × 45 cm, respectively.

Because the bedding fault zones and deep faults were usually unsaturated and some air bubbles may have entered the inlet and outlet chambers during the preparation of the test blocks, the test blocks were saturated before the application of seepage pressure. Saturation was achieved by flowing water with a *c.* 2 m water head through the test blocks while the air vent in the inlet chamber was open. The air vent was turned off after the water in the inlet chamber had overflowed from the air vent for 15 min.

As recommended by the Chinese coarse-grained soil seepage test standard SL237 (Nanjing Hydraulic Research Institute 1999), the *in situ* seepage tests started under a hydraulic gradient $i_0 = 0.05$. The hydraulic gradient i was increased gradually using a maximum increment $\Delta i = 0.5$ until seepage failure occurred in the test blocks. During the test, the seepage flux and the water heads at five piezometric tubes and the water temperature at the outlet chamber were measured every 30 min. Phenomena such as turbidity and bubbling within the seepage flow and the suspension of entrained fine particles in the outlet chamber were closely observed and recorded with respect to time.

The hydraulic gradient i and the seepage velocity v of the block were calculated at each staged pressure by measuring the water head and seepage flux. The hydraulic conductivity k_T of the test block at the test temperature was obtained via Darcy's law. During the tests, the mean temperature readings from the five tubes varied from 12.5 to 14.5 °C in YS1 and from 13.5 to 15 °C in YS2. The resulting value of k_T was then converted to an equivalent hydraulic conductivity at a temperature of 20 °C (denoted as k_{20}) to ensure comparability of the test results:

$$k_T = \frac{v}{i},\ k_{20} = k_T \frac{\eta_T}{\eta_{20}} \tag{1}$$

where η_T and η_{20} are the coefficients of the water dynamic viscosity at the temperatures T °C and 20 °C, respectively.

Test results

Figure 8 shows the results of the two *in situ* tests with respect to the change in the hydraulic gradient with the seepage velocity and the hydraulic conductivity on a log–log plot. The YS1 test was repeated twice because some cracks formed in the sealing concrete surrounding the block during the test. Small hydraulic gradients were measured between piezometric tubes 1 and 2 in the YS1 test. This indicates that the fractures may be well developed and that the seepage channel is interconnected near the inlet chamber. Therefore the hydraulic gradients in Figure 8a, b were calculated from measurements of piezometric tubes 2 and 5 and the corresponding seepage length. In Figure 8a, b, curves A and B represent the results of the two YS1 tests performed before and after the reinforcement of the test block sealing concrete, respectively. The hydraulic gradient i increases along curve A in Figure 8a almost linearly on a log–log scale with the seepage velocity v from point A_1 to point A_{11}. The hydraulic gradient i is 2.5 at point A_{11}. When the hydraulic gradient i increases from 2.5 to 3.0 (point A_{11} to point A_{12}), the seepage velocity v decreases slightly, indicating that a change in the internal structure of the block may have occurred and some fine particles may have started to move along the seepage direction. The average hydraulic gradient at points A_{11} and A_{12} (2.75) may be regarded as the critical hydraulic gradient i_c. After point A_{12}, the hydraulic gradient i increases further with the seepage velocity v until it reaches 6.0 at point A_{18}, where the sealing concrete of the test block cracked and the test was stopped. Figure 8b, shows that the

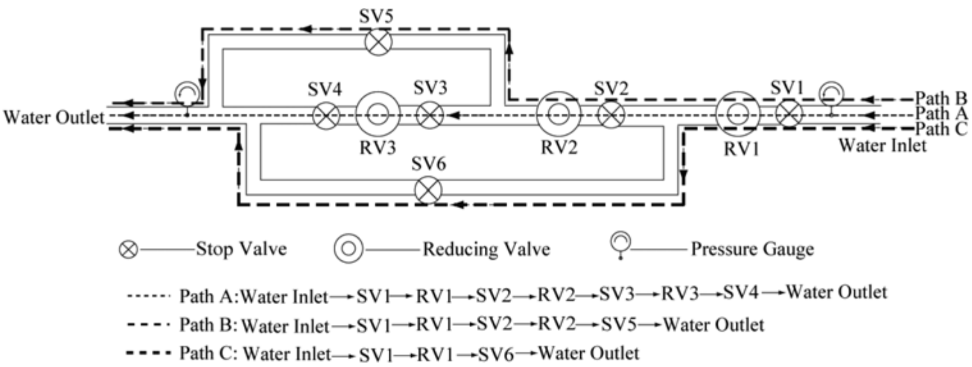

Fig. 4. The three paths in the water pressure regulating system.

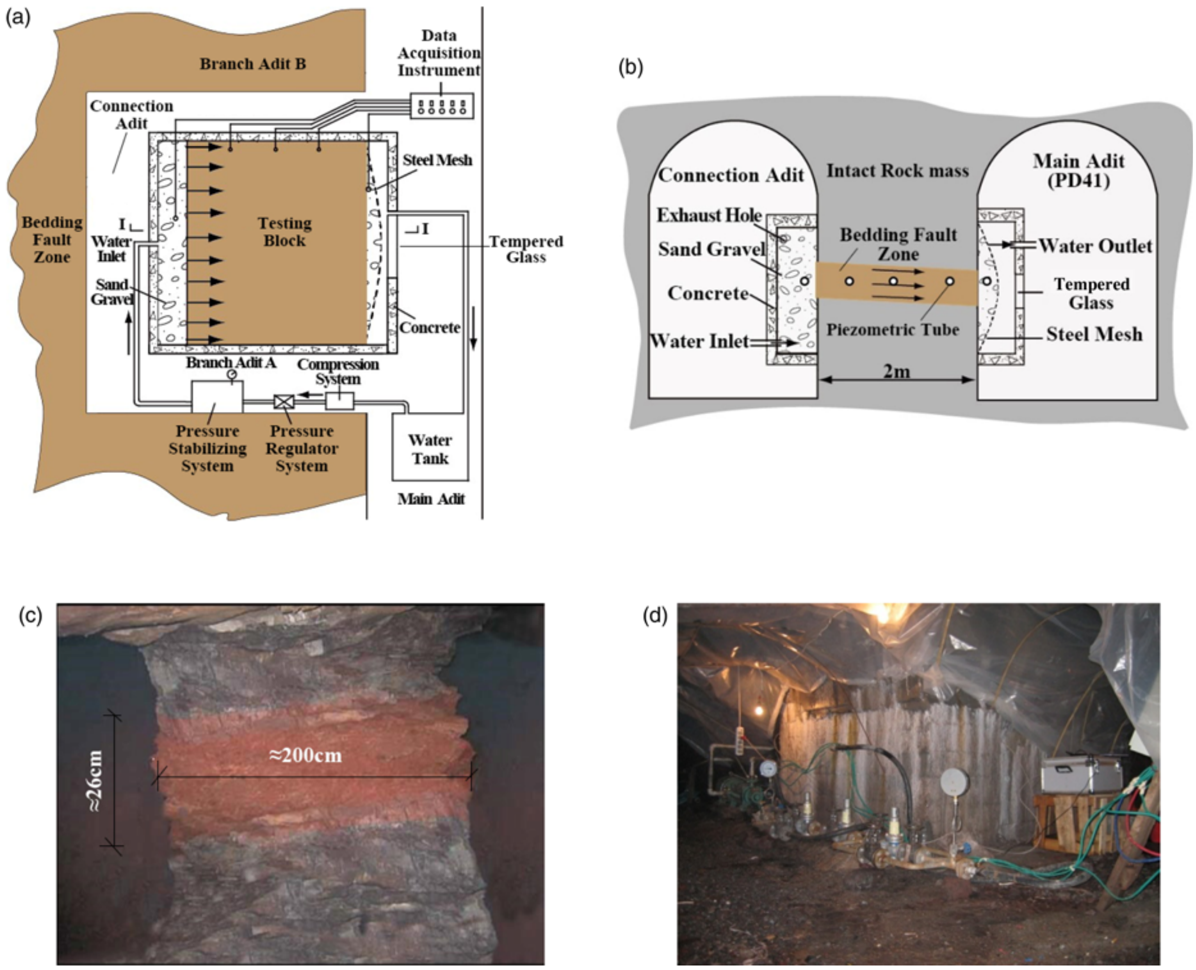

Fig. 5. Schematic diagram of the *in situ* seepage testing of gently dipping bedding fault zones: (**a**) overall arrangement (plan view); (**b**) I–I section (cross-section); (**c**) YS1 test block (front view); and (**d**) completion of the *in situ* block (YS1).

hydraulic conductivity of the YS1 test block changes slightly (ranging from 0.018 to 0.023 cm s^{-1}) before point A_{11}. The hydraulic conductivity decreases after point A_{11} as the result of an increase in fine particles along the seepage path. The hydraulic conductivity increases suddenly at point A_{18} when the sealing concrete of the block cracks.

Figure 8a, b shows that the evolution of curve B is similar to that of curve A for the YS1 test block. However, both the seepage velocity and the hydraulic conductivity in curve B are slightly smaller than in curve A under the same hydraulic gradient because the partial seepage channel is blocked by fine particles from the first test. The seepage flow increases rapidly when the hydraulic gradient i reaches 12.50 at point B_{31} and fine particles are observed to flow out of the block to the outlet chamber. The average hydraulic gradient at points B_{30} and B_{31} is therefore regarded as the failure hydraulic gradient i_F, which is equal to 12.25.

Because the internal structure of the test block may change after the critical hydraulic gradient i_c is reached, the hydraulic

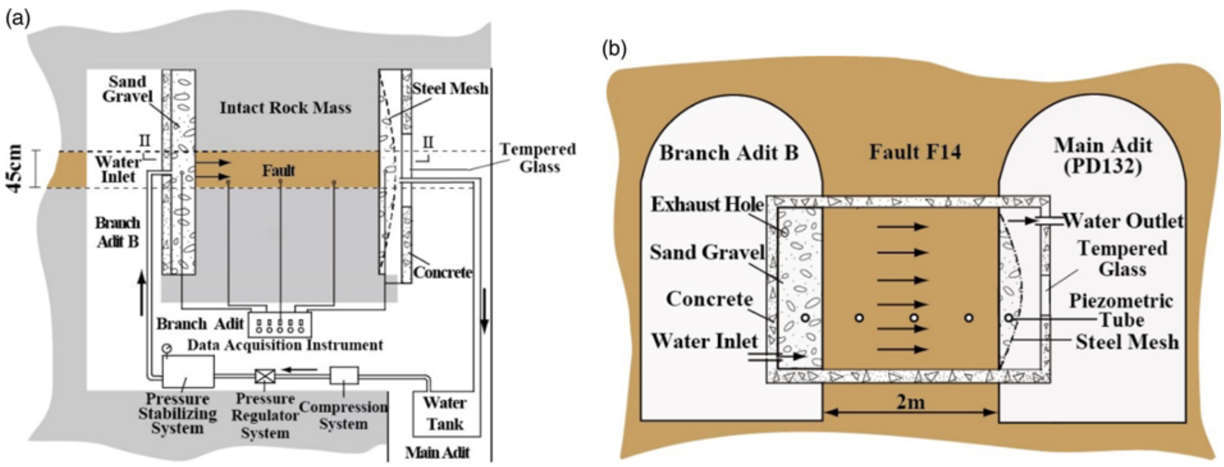

Fig. 6. Schematic diagram of the *in situ* seepage testing of steep faults: (**a**) YS2 block (plan view); and (**b**) II–II section (cross-section).

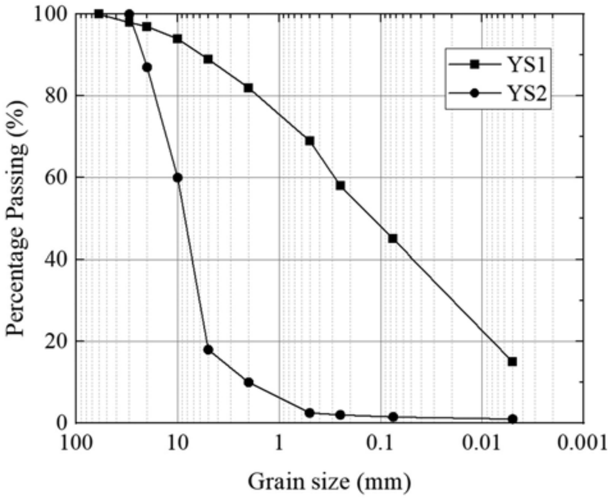

Fig. 7. Grain size distributions in YS1 and YS2 tests.

conductivity of the test block should be measured before the test. The hydraulic conductivity of the YS1 block should therefore be taken from curve A in Figure 8b. The result determined by averaging the values from points A_1 to A_{11} is *c.* 2.13×10^{-2} cm s^{-1}.

For the YS2 test block, Figure 8c shows that the hydraulic gradient i increases almost linearly on a log–log scale with the seepage velocity v from points D_1 to D_9. During the YS2 test, the water level in the inlet chamber begins to fluctuate and the seepage flow increases slightly when the hydraulic gradient reaches 2.0 at point D_9. Some fine particles flow out of the YS2 test block when the hydraulic gradient increases from 2.0 to 8.5 (from points D_9 to D_{22}) and the seepage water becomes turbid. However, the seepage water gradually changes from turbid to clear and the seepage flow decreases from points D_{22} to D_{46}. This indicates a decrease in the number of fine particles flowing out of the block and the formation of a new stable internal structure inside the block. Further increases in the hydraulic gradient result in the remobilization of the fine particles. When the hydraulic gradient reaches 48.0 at point D_{101}, the water level in the inlet chamber varies greatly and highly granular fine particles flow out of the block, together with a sudden increase in seepage flow. This leads to seepage failure of the test block.

The fine particles begin to move at point D_9 alongside pronounced changes in the slopes of both the lg$i$–lg$v$ and the lg$i$–lgk_{20} curves in Figure 8c, d. The critical hydraulic gradient of the YS2 block is taken as 2.25, which is the average of points D_9 and D_{10}. Accordingly, the hydraulic conductivity k_{20} is taken as the average value before point D_9 (i.e. 4.23×10^{-4} cm s^{-1}). The failure hydraulic gradient of the YS2 test block is taken as 47.75, which is the average of points D_{100} and D_{101}.

The hydraulic properties of rock mass discontinuities are significantly influenced by their voids, grain sizes and gradations. It is usually assumed that the internal structure of the block starts to change when the hydraulic gradient reaches a critical value. Because the filling materials within the YS2 test block are relatively uniform with a coefficient of uniformity $C_u = 4$ and the fine particle content (d<0.1 mm) is <5%, the skeleton pores formed by coarse particles cannot be completely filled by fine particles. As a consequence, fine particles are more likely to migrate in the skeleton pores under

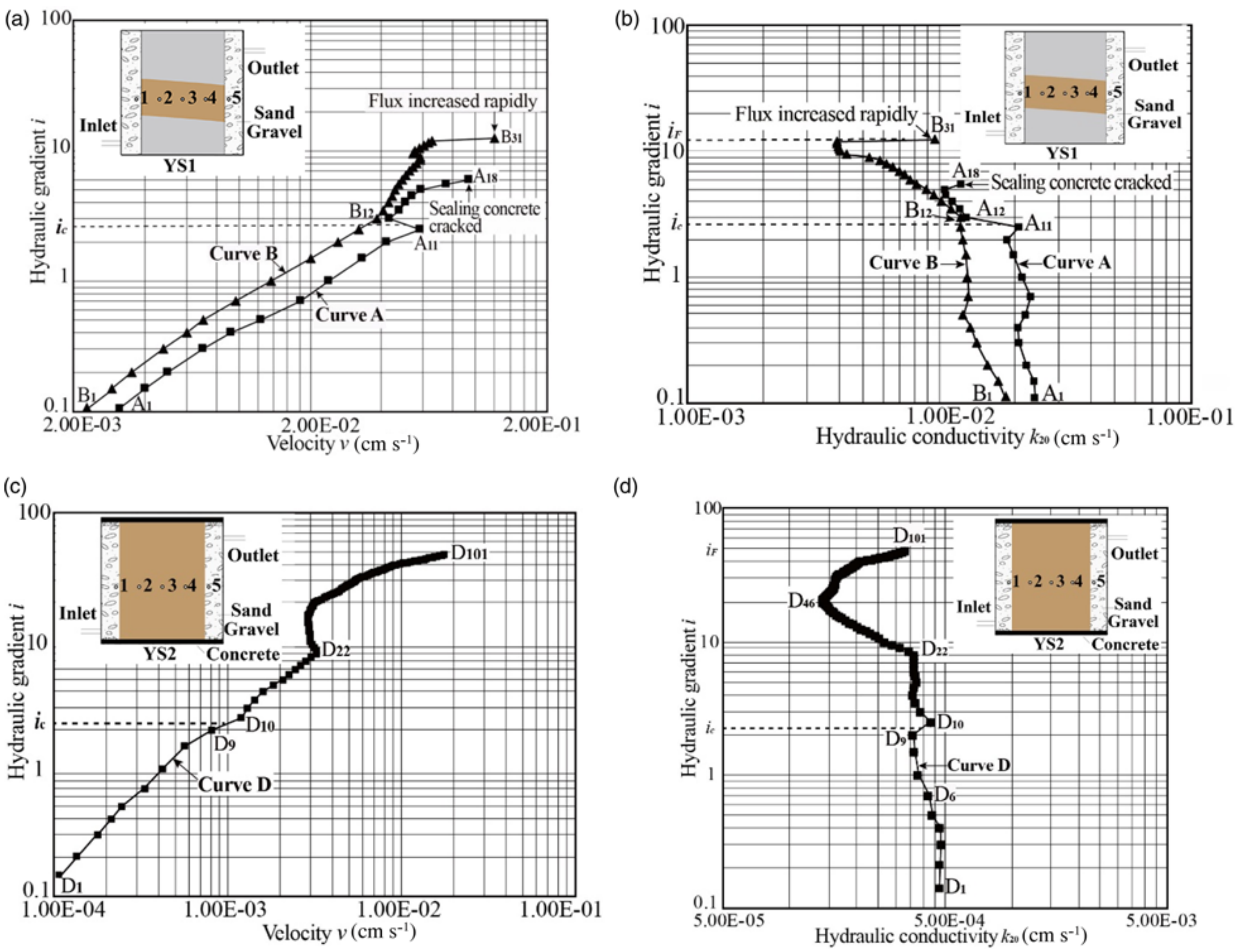

Fig. 8. Results of the YS1 and YS2 tests: (**a**) lg$i$–lg$v$ of the YS1 test; (**b**) lg$i$–lgk_{20} of the YS1 test; (**c**) lg$i$–lg$v$ of the YS2 test; and (**d**) lg$i$–lgk_{20} of the YS2 test.

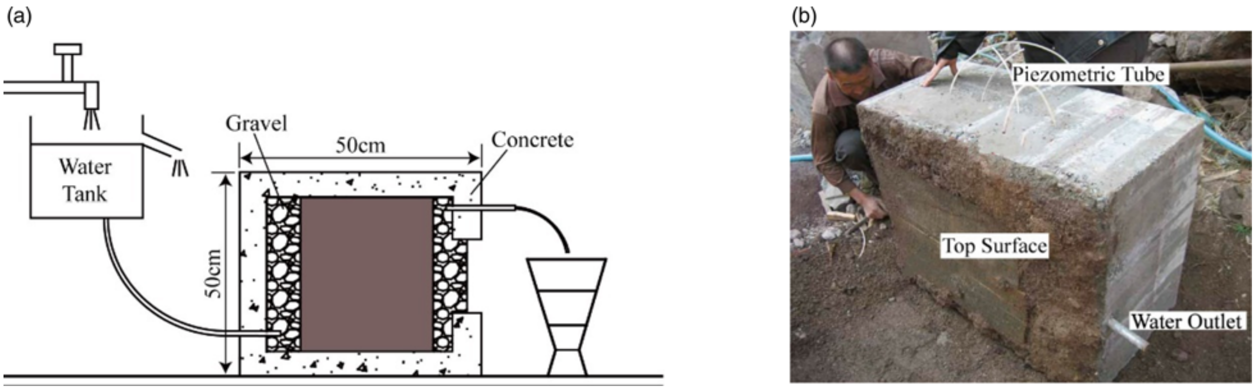

Fig. 9. Tests on undisturbed specimens: (**a**) schematic view; and (**b**) photograph of an undisturbed specimen.

seepage pressure, leading to a critical hydraulic gradient lower than that of the YS1 test block. It is easy to understand that the hydraulic conductivity of the YS1 block is greater than that of the YS2 block because the natural void ratio of the filling materials in the YS1 test block exceeds that of the YS2 test block,.

The measured seepage velocities v at points A_{18} and D_{101} are 0.098 and 0.0177 cm s^{-1}, respectively. The Reynolds numbers R_e of the YS1 and YS2 test blocks are calculated to be 86.21 and 15.53, respectively, based on the assumption that the kinematic viscosity of water is 1.31×10^{-6} m^2 s^{-1}. This shows that the seepage flow in both the YS1 and YS2 blocks is laminar and Darcy's law holds.

Comparison with seepage tests on undisturbed and reconstituted specimens

Two undisturbed specimens were taken near the test site after the YS1 test. Seepage deformation tests (UT1-1 and UT1-2) were conducted on these specimens outside the adit. The surfaces of the undisturbed specimens were first levelled by cutting and then sealed with *c.* 10 cm thick reinforced concrete. The completed specimen is 50 cm × 50 cm × 50 cm (Fig. 9). Laboratory tests were performed on a reconstituted specimen (RT1) with the same gradation composition and density as the YS1 block. The reconstituted specimen is 10 cm in diameter and 12 cm in height.

The test results Figure 10 and Table 1 show that the critical and failure hydraulic gradients are smallest and the permeability coefficients are largest in the reconstituted specimen because the natural structures of the C3 zone are completely destroyed in the reconstituted specimens and the test conditions, such as the specimen composition and the confining stress, are different from those used in the YS1 test. The critical hydraulic gradients of the undisturbed specimens are smaller than those from the YS1 test, but larger than those for the reconstituted specimen. The critical hydraulic gradient usually corresponds to the start of seepage deformation. Because seepage deformation may be considered to result from soil–rock mass instability under seepage pressure, it is influenced by the internal structures of the soil–rock mass and the restraint stress of the surrounding rock mass. The soil–rock mass is less permeable under a high restraint stress as a result of strong interactions between grains. The restraint stress of the surrounding rock mass is relieved in tests of undisturbed specimens, although the internal structures are not destroyed. As a consequence, seepage deformation easily occurs in undisturbed specimens and requires a smaller critical hydraulic gradient than that noted during the *in situ* tests. Table 1 shows that the failure hydraulic gradient i_F of undisturbed specimens taken from the same site differ significantly because of the relatively small scales of the specimens and the varying fracture distributions inside them.

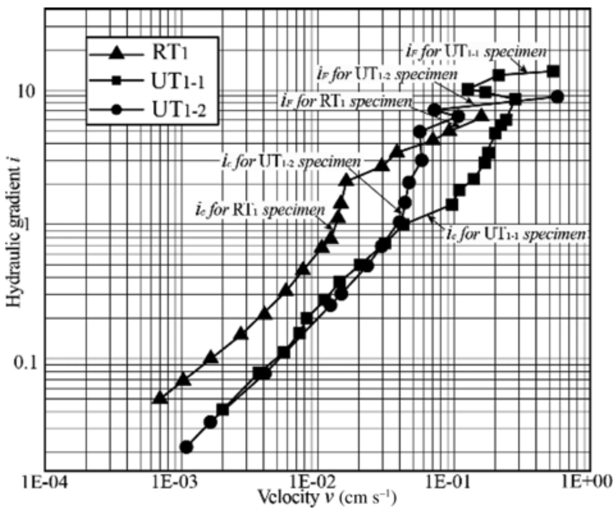

Fig. 10. Results of seepage tests on reconstituted and undisturbed specimens.

Table 1. *Comparison of seepage parameters from various tests*

Test	Critical hydraulic gradient i_c	Failure hydraulic gradient i_F	Permeability coefficient k_{20} (cm s^{-1})
YS1	2.75	12.25	2.13×10^{-2}
UT1-1	1.20	13.34	3.76×10^{-2}
UT1-2	1.28	8.00	3.43×10^{-2}
RT1	0.95	5.56	4.35×10^{-2}

Conclusions

This study introduced an *in situ* seepage testing method for large-scale rock mass discontinuities. Two *in situ* tests were performed on a gently dipping structural surface (C3 zone) and a steep fault (F14) at the Baihetan dam site. The *in situ* test results were compared with those of the undisturbed and reconstituted specimens. The following conclusions can be drawn.

(1) The proposed *in situ* seepage testing method has two advantages: the stress environment of the test block approaches natural conditions and the large test block dimensions make it more representative of rock mass discontinuities. It can therefore more reasonably be used to determine the seepage properties of discontinuous structural planes.

(2) The critical hydraulic gradients of the undisturbed specimens are smaller than those measured via *in situ* tests because the natural stress of the surrounding rock mass cannot be reflected in tests of

undisturbed specimens. The hydraulic gradients obtained are smallest when the internal structures are destroyed and natural stresses are relieved in the reconstituted specimens.

We determined the initial seepage pressure and the pressure increment applied to the test blocks during *in situ* seepage tests based on the porous media test standard. However, because the fluid flow in fractured rock is critically different from the flow in conventional porous media, the initial seepage pressure and the pressure increments can be increased in further studies. The test procedures and devices for this new method require standardization.

Acknowledgements Special thanks are extended to Xu Jianrong, Tang Mingfa, Wang Xuyun and Xu Gaofeng of Power China Huadong Engineering Corporation for valuable discussions and excellent support.

Author contributions **SL**: conceptualization (lead); **SX**: data curation (lead), writing – original draft (equal); **BZ**: project administration (lead), writing– original draft (equal).

Funding This work was supported by The Joint Funds of the National Natural Science Foundation of China (Grant No. U1765205) and the National Key R&D Program of China (Grant No. 2017YFC0404801).

Data availability statement All data generated or analysed during this study are included in this published article (and its supplementary information files).

Scientific editing by Stuart Millis; Lei Huang

References

Afrouz, A. 1992. *Practical Handbook of Rock Mass Classification Systems and Modes of Ground Failure*. CRC Press.

Cook, P. 2000. In situ pneumatic testing at Yucca Mountain. *International Journal of Rock Mechanics and Mining Sciences*, **37**, 357–367, https://doi.org/10.1016/S1365-1609(99)00111-2

Cosenza, P., Ghoreychi, M., Bazargan-Sabet, B. and De Marsily, G. 1999. In situ rock salt permeability measurement for long term safety assessment of storage. *International Journal of Rock Mechanics and Mining Sciences*, **36**, 509–526, https://doi.org/10.1016/S0148-9062(99)00017-0

Feng, S.R., Zhao, H.B., Jiang, Z.M. and Zeng, X.X. 2012. Experimental study on seepage failure characteristics of broken rock mass in dam foundation at left bank of Xiangjiaba Hydropower Project. *Chinese Journal of Geotechnical Engineering*, **34**, 600–605 [in Chinese].

Gutiérrez, F., Mozafari, M., Carbonel, D., Gómez, R. and Raeisi, E. 2015. Leakage problems in dams built on evaporites. The case of La Loteta Dam (NE Spain), a reservoir in a large karstic depression generated by interstratal salt dissolution. *Engineering Geology*, **185**, 139–154, https://doi.org/10.1016/j.enggeo.2014.12.009

Hsieh, P.A., Neuman, S.P., Stiles, G.K. and Simpson, E.S. 1985. Field determination of the three-dimensional hydraulic conductivity tensor of anisotropic media: 2. Methodology and application to fractured rocks. *Water Resources Research*, **21**, 1667–1676, https://doi.org/10.1029/WR021i011p01667

Huang, L., Tang, H., Wang, L. and Juang, C.H. 2019. Minimum scanline-to-fracture angle and sample size required to produce a highly accurate estimate of the 3-D fracture orientation distribution. *Rock Mechanics and Rock Engineering*, **52**, 803–825, https://doi.org/10.1007/s00603-018-1621-z

Huang, L., Juang, C.H. and Tang, H. 2020*a*. Assessing error in the 3D discontinuity-orientation distribution estimated by the Fouché method. *Computers and Geotechnics*, **119**, 103293, https://doi.org/10.1016/j.compgeo.2019.103293

Huang, L., Su, X. and Tang, H. 2020*b*. Optimal selection of estimator for obtaining an accurate three-dimensional rock fracture orientation distribution. *Engineering Geology*, **270**, 105575, https://doi.org/10.1016/j.enggeo.2020.105575

Jiang, Z., Sheng, F.U., Shanggao, L.I., Dake, H. and Shurong, F. 2007. High pressure permeability test on hydraulic tunnel with steep obliquity faults under high pressure. *Chinese Journal of Rock Mechanics and Engineering*, **26**, 2318–2323 [in Chinese].

Louis, C. 1972. Rock hydraulics. *In*: Müller, L. (ed.) *Rock Mechanics*. Springer, 299–387.

Louis, C. and Maini, Y.N. 1970. *Determination of In-situ Hydraulic Parameters in Jointed Rock*. Rock Mechanics Research Report, **10**. Imperial College of Science and Technology.

Mehr, S.S. and Raeisi, E. 2018. Investigation of seepage flow path(s) in the right embankment of Sheshpeer Dam, the Zagros Region, Iran. *Carbonates and Evaporites*, **34**, 1321–1331, https://doi.org/10.1007/s13146-018-0426-1

Min, K.B., Jing, L. and Stephansson, O. 2004. Determining the equivalent permeability tensor for fractured rock masses using a stochastic REV approach: method and application to the field data from Sellafield, UK. *Hydrogeology Journal*, **12**, 497–510, https://doi.org/10.1007/s10040-004-0331-7

Misstear, B., Banks, D. and Clark, L. 2006. *Water Wells and Boreholes*. Wiley.

Nanjing Hydraulic Research Institute 1999. *Specification of Soil Test SL237*. China Water and Power Press [in Chinese].

Nastev, M., Savard, M.M., Lapcevic, P., Lefebvre, R. and Martel, R. 2004. Hydraulic properties and scale effects investigation in regional rock aquifers, south-western Quebec, Canada. *Hydrogeology Journal*, **12**, 257–269, https://doi.org/10.1007/s10040-004-0340-6

Rochim, A., Marot, D., Sibille, L. and Thao Le, V. 2017. Effects of hydraulic loading history on suffusion susceptibility of cohesionless soils. *Journal of Geotechnical and Geoenvironmental Engineering*, **143**, 4017025, https://doi.org/10.1061/(ASCE)GT.1943-5606.0001673

Sato, M. and Kuwano, R. 2015. Suffusion and clogging by one-dimensional seepage tests on cohesive soil. *Soils and Foundations*, **55**, 1427–1440, https://doi.org/10.1016/j.sandf.2015.10.008

Sivakumar, S., Begum, N.A. and Premalatha, P.V. 2018. Numerical study on deformation of diaphragm cut off walls under seepage forces in permeable soils. *Computers and Geotechnics*, **102**, 155–163, https://doi.org/10.1016/j.compgeo.2018.06.015

Yamaguchi, Y., Shibuichi, H. and Matsumoto, N. 1997. Permeability evaluation of jointed rock masses using high viscosity fluid tests. *International Journal of Rock Mechanics and Mining Sciences*, **34**, 344e1–344e15.

Zhou, Z.F., Yang, J. and Yang, J.H. 1999. A field test method for determining permeability parameters of gently dipping structural face in rockmass. *Journal of Engineering Geology*, **7**, 375–379 [in Chinese].